

Massive black hole and gas dynamics in galaxy nuclei mergers. I. Numerical implementation

Alessandro Lupi¹, Francesco Haardt^{1,3} & Massimo Dotti^{2,3}.

¹*DiSAT, Università degli Studi dell'Insubria, Via Valleggio 11, 22100 Como, Italy*

²*Dipartimento di Fisica, Università degli Studi di Milano-Bicocca, Piazza della Scienza 3, Milano 20126, Italy*

³*INFN, Sezione di Milano-Bicocca, Piazza della Scienza 3, 20126 Milano, Italy*

Draft July 2014

ABSTRACT

Numerical effects are known to plague adaptive mesh refinement (AMR) codes when treating massive particles, e.g. representing massive black holes (MBHs). In an evolving background, they can experience strong, spurious perturbations and then follow unphysical orbits. We study by means of numerical simulations the dynamical evolution of a pair MBHs in the rapidly and violently evolving gaseous and stellar background that follows a galaxy major merger. We confirm that spurious numerical effects alter the MBH orbits in AMR simulations, and show that numerical issues are ultimately due to a drop in the spatial resolution during the simulation, drastically reducing the accuracy in the gravitational force computation. We therefore propose a new refinement criterion suited for massive particles, able to solve in a fast and precise way for their orbits in highly dynamical backgrounds. The new refinement criterion we designed enforces the region around each massive particle to remain at the maximum resolution allowed, independently upon the local gas density. Such maximally-resolved regions then follow the MBHs along their orbits, and effectively avoids all spurious effects caused by resolution changes. Our suite of high resolution, adaptive mesh-refinement hydrodynamic simulations, including different prescriptions for the sub-grid gas physics, shows that the new refinement implementation has the advantage of not altering the physical evolution of the MBHs, accounting for all the non trivial physical processes taking place in violent dynamical scenarios, such as the final stages of a galaxy major merger.

Key words: black hole - galaxy formation - galaxy evolution.

1 INTRODUCTION

Mergers of gas-rich galaxies are key events in hierarchical clustering models of cosmic structure formation. Galaxy mergers are thought to (*i*) be responsible of the formation of classical bulges (e.g. Kormendy 2013, and references therein), (*ii*) trigger intense bursts of nuclear star formation and AGN emission (e.g. Di Matteo, Springel & Hernquist 2005; Daddi et al. 2010; Genzel et al. 2010) with possible dual AGN activity (e.g. Callegari et al. 2009, 2011; Van Wassenhove et al. 2012; Blecha, Loeb & Narayan 2013), (*iii*) trigger the formation of massive black holes (MBH), possibly via direct collapse of gas (Mayer et al. 2010; Bonoli, Mayer & Callegari 2014), or inducing the collapse of pre-existing nuclear stellar clusters (Davies, Miller & Bellovary 2011; Lupi et al. 2014), and (*iv*) build up a population of MBH binaries (MBHBs) (e.g. Colpi & Dotti 2011, and references therein for a detailed discussion), the main targets for future campaigns

aimed at the detection of low-frequency gravitational waves (Consortium et al. 2013; Hobbs et al. 2010).

When simulating MBHs in galaxy mergers, a detailed treatment of the dynamics is of foremost importance, since it influences the MBH ability to accrete gas (hence, its mass evolution and possible onset of AGN activity), the MBH spin evolution (e.g. Dotti et al. 2010), and the formation and fate of MBHBs. The many physical processes involved require a detailed modelling of the dynamics of gas, stars, dark matter and MBHs though, hence calling for high-resolution hydrodynamical simulations.

Hydro simulations can be divided into two classes: smoothed particle hydrodynamics (SPH), in which the distribution of gas is sampled by a number of particles, and grid codes, in which the gas properties are mapped on a geometrical grid. SPH codes do not assume any a priori geometry, and automatically allow larger resolution in denser regions. Therefore, SPH codes are extensively used in galaxy

arXiv:1410.0959v2 [astro-ph.GA] 30 Dec 2014

merger simulations (see Dotti, Sesana & Decarli 2012, and references therein).

Grid codes, in order to achieve high resolution only in a limited volume of the simulation, can refine the mesh when and where required by specified properties of the fluid (adaptive mesh refinement, AMR Berger & Olinger 1984; Berger & Colella 1989). As an example, AMR allows to evolve the dynamics of gas close to MBHs, and then, e.g., determine whether AGN activity is to be expected or not, without increasing dramatically the total numbers of grids and the computational cost of the run. In principle, one can tailor the refinement criteria to obtain a super-Lagrangian increase on the resolution, allowing, e.g., for a better description of MBH sinking in late stages of galaxy mergers (see Chapon, Mayer & Teyssier 2013). Moreover, the resolution of the gravitational interaction depends on the degree of refinement, and can change and increase as the simulation proceeds, a feature not generally shared with SPH codes.

Thanks to AMR, a number of grid-based hydro simulations of the last stages of galaxy mergers have been performed to date (Chapon, Mayer & Teyssier 2013; Dubois et al. 2014). The two papers assume quite different prescriptions. Chapon, Mayer & Teyssier (2013) assume a smoother IGM, not affected by cooling, star formation (SF) and supernova (SNa) feedback, while these effects are considered in Dubois et al. (2014). In Chapon, Mayer & Teyssier (2013) the MBH dynamics depends strongly on the maximal resolution of the simulation. In lower resolution runs ($\Delta x_{\min} = 3$ pc) the MBH evolution is significantly slower (because of the underestimated effect of the resolution dependent dynamical friction), and considerably more noisy (well above the resolution level) than in the higher resolution cases ($\Delta x_{\min} = 0.1$ pc). A similar noisy evolution of the MBH orbits has been observed by Dubois et al. (2014). In order to prevent spurious oscillations of the MBH due to finite resolution effects, the authors introduced an additional drag force onto the MBHs.

Interestingly, a noisy evolution of collisionless particle dynamics (and, in particular, of MBHs) has been observed in high-resolution AMR simulations of single isolated galaxies, in which the gas is only subject to internal processes such as star formation, SNa feedback, etc. (e.g. Gabor & Bournaud 2013). In their work, in order to limit numerical MBH wandering, the authors propose two different approaches. The first one consists in modelling the MBH as an extended spherical structure, using few thousands evolving particles. Such BH-forming particles are regenerated over a secondary, coarse time grid. In this case the MBH moves out of the geometrical centre of the galaxy by hundreds to thousands of pc depending on the amount of gas simulated and the noisy effect is only reduced. The second one, instead, consists in adding an artificial velocity component directed toward the stellar centre of mass, which forces the MBH to orbit close to the galaxy centre.

As noted by Gabor & Bournaud (2013), the noisy evolution of the MBH can be either numerical (due to the limited and time varying spatial resolution), or physical, if caused by interactions with massive and dense gas clouds. This last possibility is particularly interesting when the gas is allowed to cool and actually form significant compact overdensities, as in the simulations discussed in Gabor & Bournaud (2013) and Dubois et al. (2014). Indeed,

a physically motivated noisy orbital evolution of MBHs is observed in SPH simulations (see e.g. Fiacconi et al. 2013, for a detailed and extensive discussion). It is important to notice that the effects of massive gas clumps on the MBH dynamics is severely altered by the corrections proposed in works discussed above.

This is the first of a series of papers devoted at the study of MBHB dynamics in the final stages of galaxy mergers. Here, we focus on the technical aspects of numerical simulations of the physical system under scrutiny, and propose a new adaptive refinement criterion for AMR codes, suited to properly treat the physical interactions between the MBHs and the gas clouds forming in the environment. In forthcoming papers we will exploit our newly designed simulations, exploring the parameters space, and addressing the many diverse astrophysical and cosmological consequences.

The paper is organised as follows. In Section 2 we introduce the code we developed to build our initial conditions, the simulations we have ran, and our new implementation of an evolving geometrical refinement that we implemented on the AMR code RAMSES (Teyssier 2002), in Section 3 we present the results of our test runs and compare them to results obtained without implementing our new refinement criterion. The conclusions are drawn in Section 4.

2 NUMERICAL METHODS

2.1 Initial conditions

We simulated the merger of two circum-nuclear discs (CNDs) embedded in stellar nuclei, each hosting a MBH. Such system should be considered as an idealised model of the latest stages of a galaxy merger. We initially set each of the two merging nuclei in dynamical equilibrium, and assumed they are constituted by three different components:

- a stellar spherical structure (termed “nucleus” hereinafter) described by an Hernquist profile (Hernquist 1990), defined in spherical coordinates as

$$\rho_b(r) = \frac{M_b}{2\pi} \frac{a}{r(r+a)^3}, \quad (1)$$

where $\rho_b(r)$ is the density as a function of radius r , $M_b = 2 \times 10^8 M_\odot$ the total nucleus mass, and $a = 100$ pc the nucleus scale radius.

- an exponential gaseous disc with surface density profile defined in cylindrical coordinates as

$$\Sigma_d(R) = \frac{M_d}{2\pi R_d^2} \exp(-R/R_d), \quad (2)$$

where R is the disc radius, $R_d = 50$ pc the disc scale radius, and $M_d = 10^8 M_\odot$ the total disc mass.

- a MBH with mass $M_{\text{BH}} = 10^7 M_\odot$, at rest in the centre of the disc.

In order to ensure equilibrium, we iteratively calculated the vertical density profile of the disc and, consequently, the velocity fields of gas and stars by means of the dedicated code GD_BASIC¹. The code samples gaseous and stellar particles, eventually used as the initial condition for the SPH

¹ The code is publicly available at <http://www.dfm.uninsubria.it/alupi/software.html>

run (see next section 2.2). GD_BASIC solves the disc hydrostatic equilibrium equations for a user-defined surface density profile subject to the additional potentials of the Hernquist nucleus and of the MBH. Defining the gas pressure as

$$P_d = (\gamma - 1)\rho_d u, \quad (3)$$

where γ and u are the gas polytropic index and internal energy respectively, and assuming a single temperature disc (in our case, we adopted an initial fiducial value of $T = 2 \times 10^4$ K), the vertical equilibrium equation can then be written as

$$\frac{1}{\rho_d(R, z)} \frac{\partial P_d(R, z)}{\partial z} = -\frac{\partial \phi(R, z)}{\partial z}, \quad (4)$$

where $\phi(R, z)$ is the global gravitational potential of the system. Using eq. 3, eq. 4 can be solved for the disc surface density:

$$\Sigma_d(R) = \rho_d(R, 0) \int_{-\infty}^{+\infty} \exp\left[-\frac{\phi_z(R, z)}{(\gamma - 1)u}\right] dz, \quad (5)$$

where $\phi_z(R, z) \equiv \phi(R, z) - \phi(R, 0)$ is the vertical component of the global potential.

We further assumed the thin disc approximation, so that the Poisson equation can be simplified to

$$\frac{\partial^2 \phi_d}{\partial z^2} + \nabla^2 \phi_b = 4\pi G[\rho_d(R, z) + \rho_b(r)], \quad (6)$$

where ϕ_d and ϕ_b are the disc and the nucleus potentials, respectively. Since $\nabla^2 \phi_b = 4\pi G\rho_b$, we can write

$$\frac{\partial^2 \phi_{d,z}}{\partial z^2} = 4\pi G\rho_d(R, z) = 4\pi G\rho_d(R, 0) \exp\left[-\frac{\phi_z(R, z)}{(\gamma - 1)u}\right], \quad (7)$$

where we defined $\phi_{d,z} \equiv \phi_d(R, z) - \phi_d(R, 0)$ as the vertical component of the disc potential.

We solved the above equations forcing the vertical hydrostatic equilibrium of the disc, assuming an exponential surface density profile as boundary condition. We started solving eq. 7 for $\phi_{d,z}$ by guessing an initial equatorial profile $\rho_d(R, 0)$. Then, we computed the total vertical potential ϕ_z , and by means of eq. 5, a new value for $\rho_d(R, 0)$ that satisfies the boundary condition Σ_d was derived. The procedure was iterated until convergence. From eq. 7 we obtained $\phi_{d,z}$ and, from eq. 4, $\rho_d(R, z)$. As in the iterative procedure $\phi_d(R, 0)$ is a free parameter, we assumed a razor thin exponential disc (equation 2-168 in Binney & Tremaine). Finally, the velocity of the disc particles was evaluated by setting the radial component of the velocity equal to 0 (hydrostatic equilibrium assures that the vertical component is null as well), while the tangential velocity was obtained from the Euler equation in the case of a rotationally supported disc.

Concerning stellar-like particles, we evaluated the distribution function f in the 6-dimensional phase-space. We initially considered the Hernquist spherical structure subject only to its own potential and to the MBH potential (i.e., $\phi = \phi_b + \phi_{\text{MBH}}$), implying that f depends only on the particle total energy in this case. From the Eddington's formula (equation 4-140a in Binney & Tremaine) we have

$$f(\epsilon) = \frac{1}{2^{3/2}\pi^2} \frac{d}{d\epsilon} \int_{\epsilon}^0 \frac{d\rho_b}{d\phi} \frac{d\phi}{(\phi - \epsilon)^{1/2}}, \quad (8)$$

where ϵ is the particle energy per unit of mass, and ρ_b can be expressed as a function of ϕ (being ϕ a monotonic function

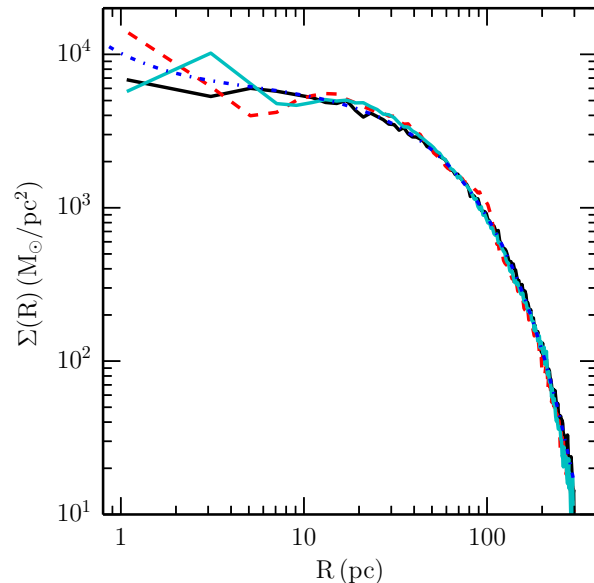


Figure 1. Surface density profile for a disc evolved in isolation using Gadget-2. The solid black, dashed red and solid cyan curves are obtained from the gas particle distribution at $t = 0, 5$ and 10 Myr, respectively. The dash-dotted blue curve is the profile calculated with the algorithm described in the text.

of r). The distribution function was numerically evaluated and used to sample the nucleus particle energy density. We then derived the particle speed $v = \sqrt{2(\epsilon - \phi)}$, where ϕ was computed at the particle position. In order to correct for the neglected contribution of the disc to the global potential, we added to the spherically symmetric component of the potential the approximate contribution of the disc in the form $\phi_d = GM_d(< r)/(3r)$, where $M_d(< r)$ is the mass of gas particles within r .

In order to test the stability of our initial conditions, we evolved each disc in isolation for 10 Myr. The evolved disc surface density is shown in fig. 1 at different times. The profile changes in the inner $\simeq 20$ pc because of a gas instability developing after $\simeq 2$ Myr from the start. In order to assess the origin of such instability, we numerically estimated the Toomre parameter of the disc Q at initial time $t = 0$ ($Q \equiv kc_s/(\pi\Sigma)$, where k is the epicyclic frequency and c_s is the gas sound speed). Note that, strictly speaking, the initialised disc is not infinitesimally thin, so that Q as defined above represents a lower limit. Fig. 2 shows the Toomre parameter at $t = 0$ as a function of the radial distance R . We found $Q > 2$ everywhere, with the notable exception of the region $10 \lesssim R \lesssim 150$ pc, where $1 \lesssim Q \lesssim 2$. The formation of transient spiral arms in this region, clearly seen during the disc evolution, suggests a genuinely physical origin of the disc instability. Such instability results in small changes in the surface density profile in the $10 \lesssim R \lesssim 150$ pc region. The system, now slightly out of equilibrium, undergoes a re-adjustment of the gas distribution down to the very central region of the disc, as observable in fig. 1 down to 5 – 10 pc from the MBH. Finally, no evidence of any fragmentation instability during the overall evolution was seen, in agreement with Q being always $\gtrsim 1$.

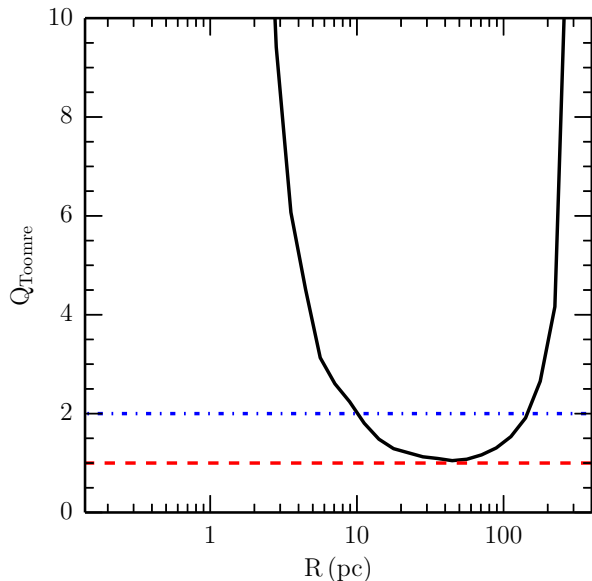


Figure 2. Toomre parameter at $t = 0$ Myr for the isolated disc using the thin disc approximation. The dashed red line corresponds to $Q = 1$, while the dash-dotted blue one to $Q = 2$. The y-axis has been limited in the interval between 0 and 10 to highlight the instability interval, corresponding to $Q < 2$. The region within the inner 1 pc is not visible because of the very large values assumed by Q , outside the axis limits considered.

2.2 Simulation suite

The procedure described above was then used to build two equal mass co-rotating discs, each described by 10^5 particles, at an initial separation of 300 pc. The initial conditions for the AMR runs have been obtained mapping the gas particle distribution on the grid using the publicly available code TIPGRID². The discs were set on an initially elliptical orbit with eccentricity $e = 0.3$ and orbital angular momentum antiparallel to the angular momentum of each disc. In order to test numerical stability and assess the reliability of the system evolution, we decided to run our simulation using two intrinsically different methodologies, using the SPH code GADGET2 (Springel 2005) and the AMR code RAMSES (Teyssier 2002), in their publicly available releases. We note that GADGET2 public version does not include gas cooling, supernova feedback and star formation, while the gas obeys a polytropic equation of state. On the contrary, the available RAMSES release includes all the mentioned physical processes (Teyssier 2002; Rasera & Teyssier 2006; Teyssier et al. 2013).

As described in §1, several past AMR simulations similar to what we present here are reported to show a noisy evolution of the orbits of the two MBHs, and different techniques have been proposed to solve the problem (Gabor & Bournaud 2013; Dubois et al. 2014). The reason behind numerical perturbations in the MBH motion lies most probably in the change of the gravitational force computation accuracy during the simulation, which is related to

Run	Cooling	Star Formation	SNa feedback	New Refinement
Plain	No	No	No	No
Plain+	No	No	No	Yes
Noblast	Yes	Yes	Yes	No
Blast	Yes	Yes	Yes	No
Blast+	Yes	Yes	Yes	Yes

Table 1. The suite of RAMSES runs.

the change in the cell size. We therefore developed a new refinement criterion aimed at ensuring a fixed accuracy when computing the gravitational force acting on the two MBHs. We implemented a new refinement criterion based on the identity and positions of selected particles, rather than on the global geometry of the system. In our new implementation, refined grids follow the positions of the two MBHs at each time-step. Surrounding cells within two specified, MBH-centered volumes are flagged for further multi-level refinement. Up to seven concentric regions of increasing resolution can be user-defined by setting the seven corresponding radii. For example, in the runs discussed in this paper we enforced the maximum level of refinement, with single cell linear sizes of 0.39 pc, within 10 pc from each MBH. At larger distances from the MBHs the resolution degrades smoothly unless another refinement criterion is matched. On the top of the newly implemented criterion discussed, we use the standard Quasi-Lagrangian and Jeans criteria already implemented in RAMSES (Teyssier 2002), as described below.

We performed a total of five simulations with RAMSES, in order to compare the new refinement criterion with the standard one, and to test the reliability of the dynamical evolution of the MBH binary under different assumptions regarding the so-called “sub-grid physics”. We also carried out a single simulation with GADGET2, assuming a polytropic equation of state with index $\gamma = 7/5$. The spatial resolution for the SPH simulation is 0.2 pc, while the mass resolution is $10^3 M_\odot$ and $2 \times 10^3 M_\odot$ for gas and collisionless particles, respectively. The maximum spatial resolution (at the highest refinement level) for all our AMR simulations is ~ 0.39 pc and the mass resolution for stars is equal to that in the SPH run. The standard Jeans criterion enforced in all the simulations (with and without our new refinement implementation) ensures that the Jeans length is resolved with at least 4 cells (14 in the highest refinement level) everywhere, so to avoid the formation of spurious clumps due to resolution limits. The Quasi-Lagrangian criterion, on the other hand, allows us to resolve a minimum gas mass of $10^3 M_\odot$ everywhere, equal to the gas particle mass used in the SPH run.” Table 1 shows the suite of RAMSES simulations with the main features highlighted.

In runs “Plain” and “Plain+” no sub-grid physics is implemented, while in the following three runs, termed “Noblast”, “Blast” and “Blast+”, we included both gas cooling and star formation (with associated SNa feedback). In these runs we assumed a density threshold for star formation (SF) of $2 \times 10^6 \text{ cm}^{-3}$, and a typical (SF) timescale of 1.0 Myr. We employed a SNa yield of 15%. The specific energy budget from SNa, $10^{50} \text{ erg}/M_\odot$, is totally released in the parent cell as thermal energy. The subsequent SNa feedback was imple-

² The code is available at http://www.astrosim.net/code/doku.php?id=home:code:analysistools:misc_tools

mented in two different ways. The first recipe (“Noblast” run) assumes that gas starts to cool down immediately after it is released in the SNa event. The second feedback scheme used in the “Blast” and “Blast+” runs (Teyssier et al. 2013) assumes that the internal energy injected by SNa is decoupled from the standard gas cooling, decaying exponentially on a timescale of 20 Myr. This second scheme implicitly assumes the presence of non-thermal processes accelerating the SNa blast wave. Such non thermal energy is characterised by much longer dissipation time-scales than the thermal component (see, e.g. Enßlin et al. 2007). We finally note that typical timescale for the onset of SNa is much longer compared to the typical gas inflow timescale in our simulations, i.e., SNa would have little/negligible effects on MBH and gas dynamics. In order to enhance feedback effects, we assumed no time delay for the onset of SNa after star formation. No AGN feedback has been included in any of the runs. Our new dynamic refinement criterion is implemented in the two “+” runs.

3 RESULTS

The upper panels of Figure 4 show the MBH pair orbit in run Plain compared to the SPH run. While the orbital evolution computed by GADGET2 shows a smooth orbital decay of the pair, run Plain shows an abrupt change in the direction of motion of the two MBHs after $\sim 2 - 3$ Myr from the beginning of the run. At this time the MBHs suddenly leave the gas (upper panels in Figure 5) and stellar overdensities they inhabited. Such an abrupt acceleration could, in principle, have a physical explanation. For example, the sudden swerve could be the outcome of short range encounters between the MBHs and compact massive clumps or stellar clusters. We note, however, that such an interpretation is unlikely because of two reasons: (*i*) a strong gravitational perturbation would have affected the gas and stellar nuclei as well as the MBHs, and (*ii*) as described in Section 2, the gaseous discs in our simulations are initially stable against fragmentation, and the gas distribution is expected to remain smooth during the entire evolution in run Plain, in which no cooling prescription is implemented. A search for gas and stellar clumps in the snapshots of run Plain confirmed this expectation.

The peculiar and unexpected dynamical evolution of the MBHs in run Plain could be a numerical artefact, due to the rapid variation of the spatial resolution around the two MBHs. Figure 3 shows the number of cells at the maximum refinement level within 5 pc from each MBH. The sudden drop of resolution is caused by a density drop during the first stages of the simulation. Such a gas readjustment is expected, since the initial conditions were stable in isolation, and the two circum-nuclear discs are initially set at a finite separation. We stress that, although this initial gas evolution is driven by the procedure used to generate the initial conditions, similar sudden resolution changes are expected also due to the evolution of the gas subject to additional physics, such as SNa explosions, as discussed below.

To check if the unexpected behaviour of the MBHs is a pure numerical effect we ran the same simulation forcing the code to keep a high resolution close to the moving MBHs, through our new refinement implementation. The MBH or-

bit evolution resulting from this check (Run Plain+) is shown in figure 4. Run Plain+ shows a dynamical evolution closer to that obtained in the SPH run, that by construction is not affected by any significant fluctuation of the gravitational spatial resolution. Figure 5 shows that with our new refinement implementation the MBHs do not decouple from the gas structure they are hosted in. We further stress that an enhanced resolution close to the MBHs would facilitate the formation of gas clumps as well as maximise the effect of their gravitational interaction (if clumps would form) with the MBHs. The absence of abrupt kicks in the MBH dynamics in run Plain+ proves that the MBH noisy motion observed in run Plain is numerical and it is caused by poor/rapidly changing resolution in the region surrounding the MBHs. Still some differences in the orbital evolution of the MBHs in run Plain+ and SPH are observable. The initial difference in the vertical motion is probably caused by the resolution increase occurring in the very early stages of the simulation, when the initial conditions (with a maximum resolution of ~ 1.5 pc) are further refined to reach the desired resolution of ~ 0.39 pc. Furthermore, the MBH orbital decay after the first 3 Myr is faster in the Plain+ run with respect to the SPH run. We checked that this is due to the different magnitude of the gas inflow toward the geometrical centre of the system. Such inflows are caused by the angular momentum removal associated with the shocks developing at the contact surface between the two merging circum-nuclear discs (CNDs). The two numerical implementations (SPH and AMR) differ significantly in their treatment of the shocks, resulting in a different MBH dynamics. The detailed discussion of the physical evolution of the system and of its effect on the pairing of the MBHs will be discussed in Lupi et al. in prep.

To study the effect of the refinement prescriptions onto the MBH dynamics in less idealised simulations, we performed three runs (Noblast, Blast and Blast+) allowing the gas to radiatively cool and form stars. As shown in the following, the orbital evolution strongly depends on the different implementation for the feedback by SNa. Figure 6 shows the MBH orbital evolution in run Noblast. The MBH dynamics does not show anything similar to the huge kicks that decouple the MBH dynamics from the gas distribution observed in run Plain. On the contrary, figure 7 demonstrates that the MBHs are still well within the gas and stellar overdensities close to the centres of the dramatically perturbed nuclear discs.

However, smaller swerves mainly limited to the disc plane are still observable in the MBH orbits (figure 6). Figure 3 demonstrates that, in run Noblast, the wiggles in the orbits are not related to a decrease of the spatial resolution. Indeed the resolution around each MBH remains almost constant during the entire run, with a high number of cells populating the maximum refinement level. Such a high resolution is ensured by the formation of high density condensation of cooling gas around the MBHs.

The peculiarities in the MBH orbits in run Noblast are due to close interactions with massive clumps, forming in the disc when the gas is allowed to cool. Indeed a large number of massive clumps form during the first stages of the merger, especially along the gas shock surface between the two gaseous discs, as observable in the left panel of figure 7. These clumps can lead to very energetic kicks to MBHs, unless they are de-

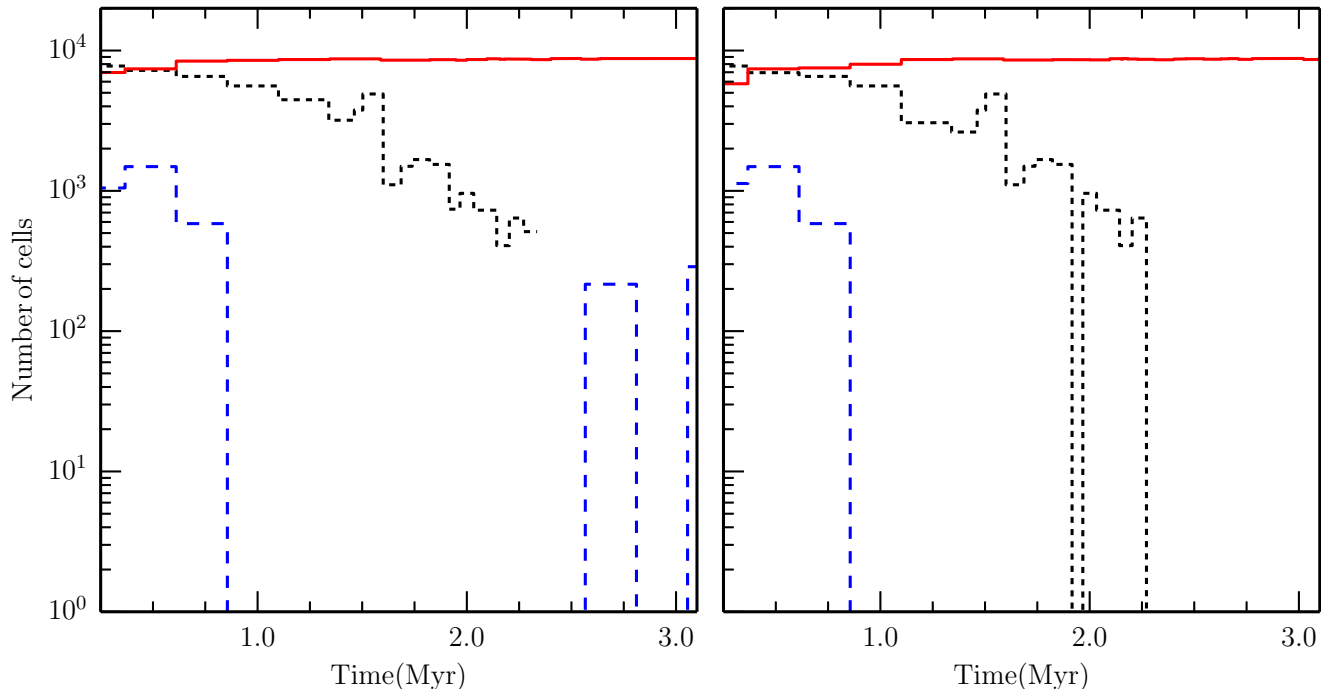


Figure 3. Number of cells for the highest refinement level around each of the two MBHs versus time for simulations Plain (blue dashed line), Noblast (red solid line) and Blast (black dotted line).

stroyed before the interaction by SNaes. This is not the case for run Noblast, in which the large thermal energy injected by SNaes in the gas immediately starts to cool, thus leaving clumps nearly unperturbed. As discussed above, this boosts the probability of having a strong cloud/MBH interaction, and results in a high resolution close to the MBHs (preventing spurious numerical wandering of the MBHs). Figure 8 highlights a strong interaction between each MBH and a massive cloud in run Noblast, taking place at $t = 5.8$ Myr. Figure 9 shows a later stage ($t = 9$ Myr) of the evolution, when the two MBHs evolve in a smoother environment. In both cases the clouds have been identified extracting the cells with a density exceeding 8×10^5 H/cc and then grouping together the adjacent cells. The detailed analysis of the interactions between MBHs and clouds as well as a broader study of the effect of the gas dynamics onto the MBH pairing is deferred to a paper in preparation.

If instead the gas is unable to rapidly get rid of the energy injected by SNaes we expect a smaller incidence of MBH-cloud interactions, but at the same time the SNaes can strongly affect the densest and intensely star-forming regions close to the MBHs. A SNa-driven gas depletion may result in a decreasing force resolution when the new refinement discussed here is not implemented. Figure 10 shows a comparison between the MBH dynamical evolution observed in runs Blast and Blast+. A peculiar wandering of the two MBHs in the three dimensions is observed in run Blast, similarly to what happens in run Plain. We stopped the run after 2 Myr only, when the MBH motion had already been affected by the numerical effect and MBHs had been scattered very far from the disc plane.

Again, the peculiar motion of MBHs in run Blast could either be a numerical artefact or have a physical origin. We

note that in both runs Blast and Blast+ the clumps are disrupted on short timescales by SNaes. Hence, gas overdensities are not expected to perturb significantly the dynamical evolution of MBHs. Furthermore, the feedback are energetic enough to deplete the gas from the nuclear regions of both discs, leaving the MBHs in an under-dense region (see figure 11). The time evolution of the number of cells at high resolution levels in the MBH vicinities is shown in Figure 3. This confirms that the energy injection from SNaes drives a significant resolution drop during the first 3 Myr, as also observed in run Plain. In run Blast, however, the loss of resolution does not directly depend on our realisation of the initial conditions, but it is a consequence of the physical evolution of the system.

The different dynamical evolution observed in run Blast+ (lower panels in figure 10) finally proves that the jerks in the MBHs paths are numerical artefacts. In fact, in this last case, the MBHs follow a very smooth evolution over multiple orbital timescales, due to the little effect of the transient gas overdensities onto the MBHs. The comparison between the results of run Blast and run Blast+ proves the effectiveness of refinement implementation discussed here in modelling massive particle dynamics in rapidly evolving backgrounds.

4 CONCLUSIONS

In this paper we propose a new refinement criterion to follow in details the motion of massive particles in AMR simulations with RAMSES. The goal of our investigation is to achieve an accurate dynamical evolution of MBHs under the

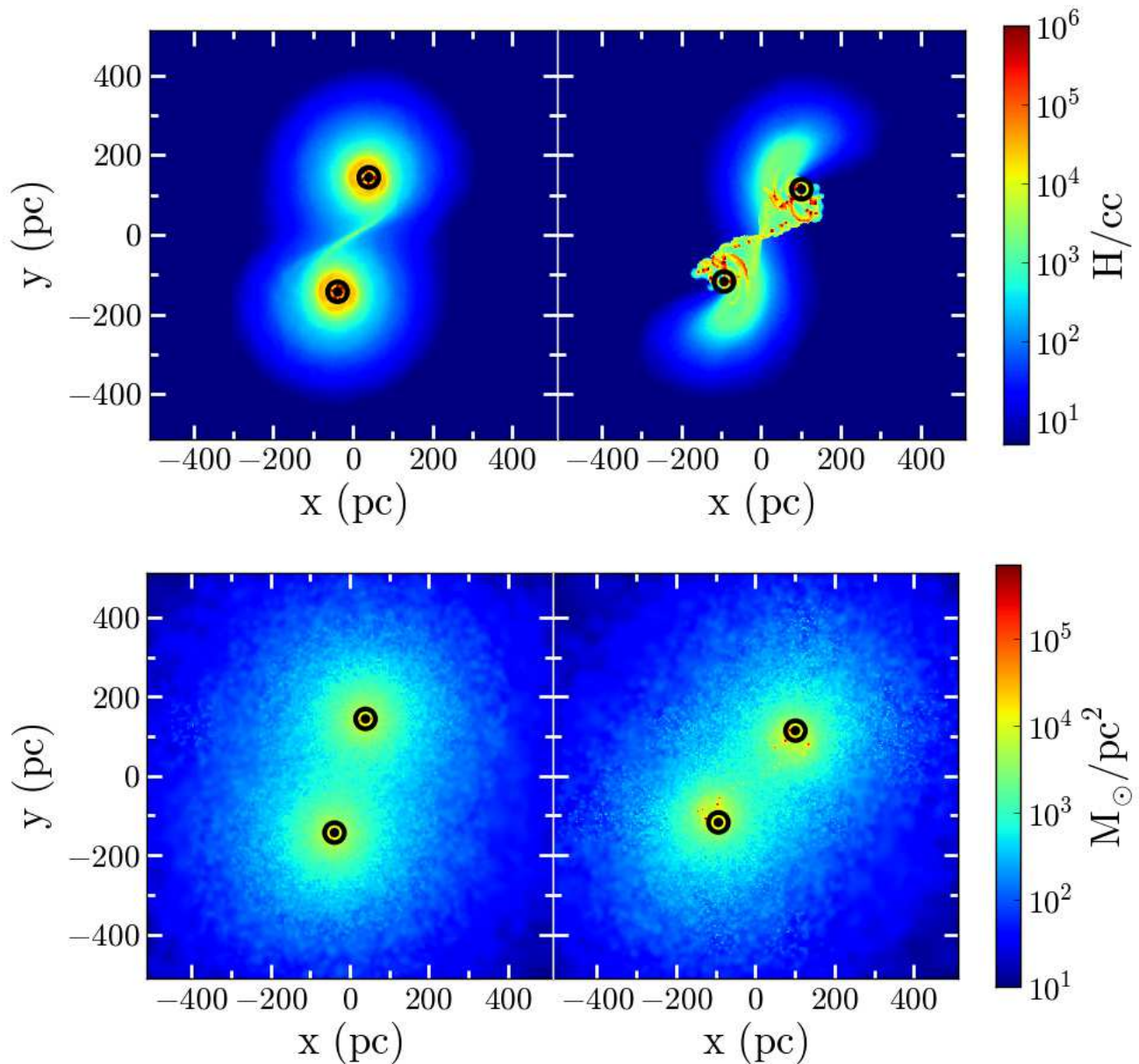


Figure 7. Upper (lower) panel: gas (stellar) density map at $t = 1$ and 3 Myr (left and right panel respectively) in run Noblast. All the notation is the same as in figure 5

influence of the evolving gaseous and stellar background, as expected in the final stages of a galaxy merger.

The accuracy in the computation of gravity force in AMR codes strictly depends on the local resolution and thus on changes in the physical properties of gas and particles during the runs. The refinement prescriptions already implemented in RAMSES do not ensure a proper description of the orbit of massive particles. Whenever the region close to the MBHs is de-refined the MBHs can experience strong spurious perturbations and then follow unphysical orbits, often leading out of the host nucleus.

We simulated the merger of two CND/stellar nucleus structures, each hosting a MBH. Such system should be considered as an idealised model of the latest stages of a galaxy merger, as we neglected possible galactic scale effects (e.g.,

large scale gas inflows). We ran a suite of simulations, including different sub-grid physics prescriptions for the gas, in order to test the changes in the MBH orbits with or without our additional refinement criterion. We demonstrated that whenever the gas density near the MBHs is reduced, the simulations run without our new implementation result in unphysical orbits. Such MBH wandering was observed in runs without gas cooling as well as in the more complex case in which the gas in the two nuclei is allowed to cool, form stars and be efficiently heated by stellar feedbacks. We stress that the complex, violent and intrinsically dynamical nature of the merger does not allow to predict whether and when a sudden drop in resolution will occur. In order to trust the simulation results a different refinement criterion, forcing a high and constant resolution near the MBHs, is required.

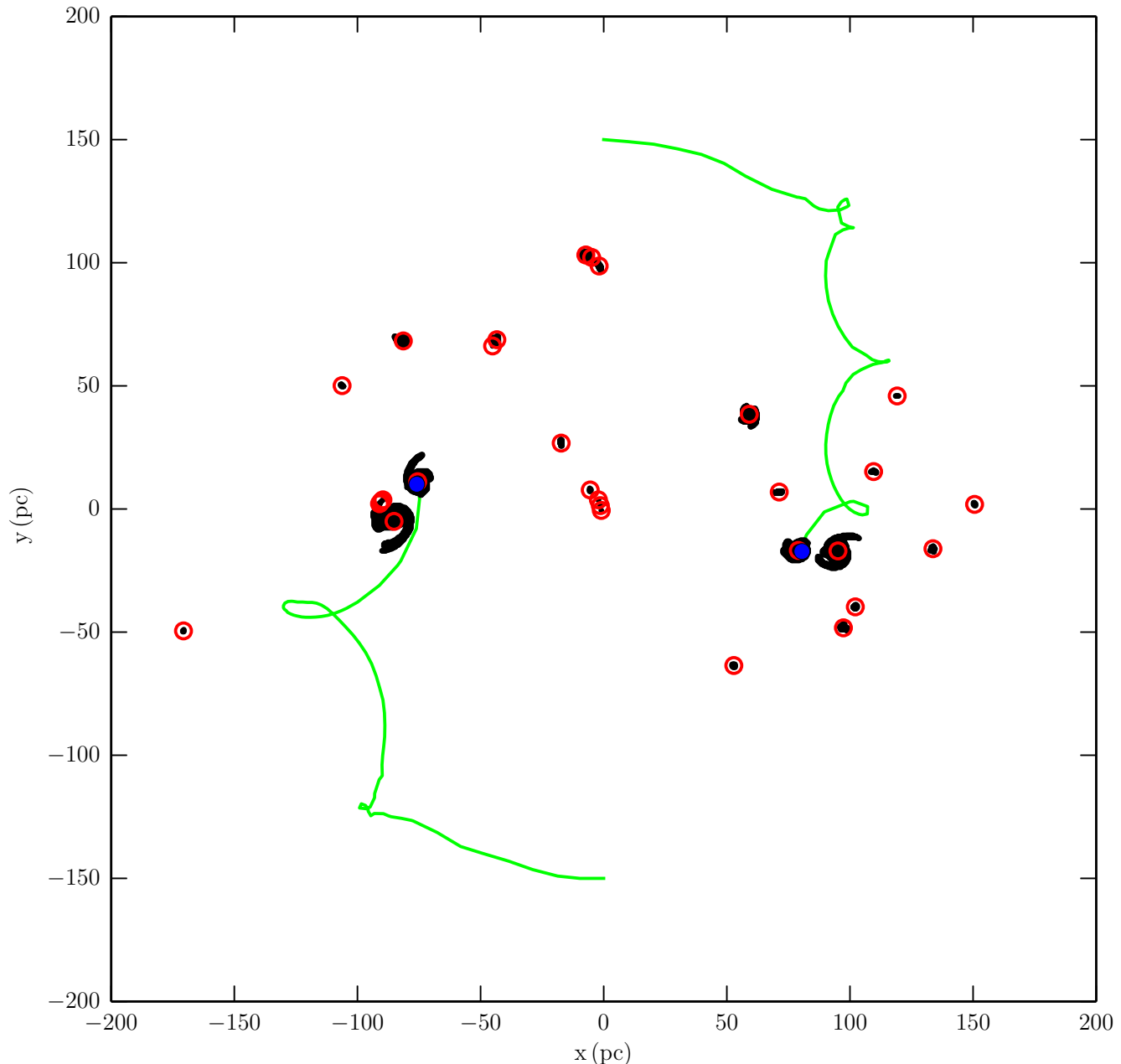


Figure 8. Strong interactions between the MBHs and massive gas clouds in run Noblast at time 5.8 Myr. The MBHs orbital path and current positions are marked with green lines and blue dots. The black regions highlight the cells forming the clouds, whose centre of mass is marked by the red empty circles (only for clouds formed by at least 10 cells).

The prescription we designed enforces the region around each massive particle to remain at the maximum resolution allowed. Such region follows the MBHs along their orbits, reducing the computational cost of the runs, and avoiding the spurious effect caused by the resolution changes.

Other possible solutions to the numerical noise of massive particle dynamics have been proposed in literature (Gabor & Bournaud 2013; Dubois et al. 2014). We stress that our implementation has the ability of not altering the physical evolution of the MBHs³. As an example, we demon-

strated that in our implementation any close interaction between the MBHs and gas clumps is properly modelled (at an equivalent/better resolution than what would be achieved without our refinement criterion). Hence, while our prescription removes the numerical effects resulting in an artificially noisy orbital evolution, it preserves all the non trivial phys-

SES has been released. In the new implementation the accelerations experienced by massive collisionless particles are computed through direct summation (R. Teyssier, private communication). The comparison between our refinement strategy and the new implementation is postponed to a future investigation.

³ During the final editing of this paper a new version of RAM-

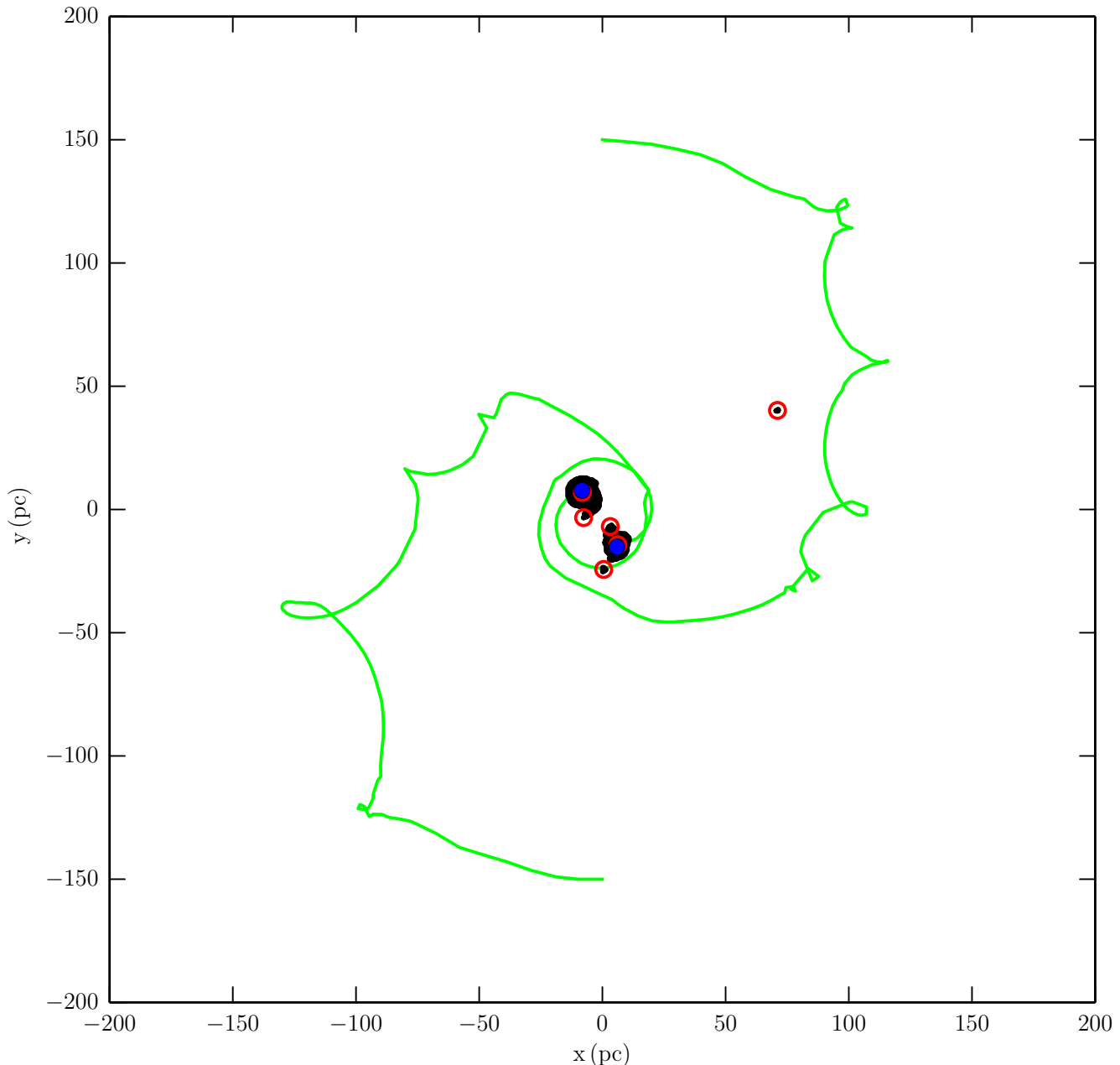


Figure 9. Same as figure 8, but at time $t = 9$ Myr. The figure shows a final stage of the orbital evolution, when the MBHs are surrounded by gas overdensities and no significant MBH/cloud interactions are taking place.

ical processes that take place in violent dynamical scenario such as the final stages of a galaxy merger.

We plan to use the new refinement criterion in a larger suite of simulations to accurately study the MBHs dynamics down to the formation of a close binary, to constrain the ability of the MBHs to accrete during their final pairing, and to properly trace the dynamics of the fuelling gas. This is important since, e.g., accreting gas affects the MBH spins and in case of mergers, the spin of the MBH remnant and its recoil velocity (see e.g. Sesana et al. 2014, and references therein). Our study will complement the AMR runs discussed in, e.g., Dubois et al. (2014); Dubois, Volonteri & Silk (2014), constraining the effect of

the MBH numerical wandering on its feeding and its spin evolution. Furthermore, the new simulation suite will serve as a comparison to similar investigations performed with SPH simulations (Escala et al. 2005; Dotti et al. 2009, 2010; Hopkins et al. 2012; Maio et al. 2013), that do not suffer the spurious MBH dynamical evolution (since the gravitational resolution is fixed in time) but that have a completely different implementation of the gas hydrodynamics.

Finally, our suite will also test whether (or under which conditions) the strong perturbations due to the merger of the two host nuclei can result in the condensation of huge and compact gas overdensities, possible progenitors

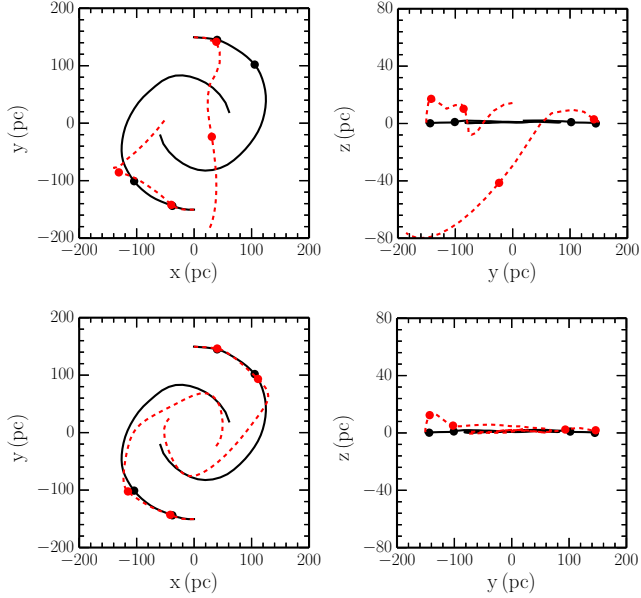


Figure 4. Orbits for the two MBHs from RAMSES runs Plain and Plain+ , compared with the SPH run. The panels on top show the orbits projected in the face-on (on the left) and edge-on (on the right) views for run Plain, plotted as red dashed lines and the SPH run, plotted as black solid lines. The panels at the bottom are the same plots obtained from run Plain+ and the SPH run. The points mark the MBH positions at $t = 1$ and 3 Myr for the runs considered.

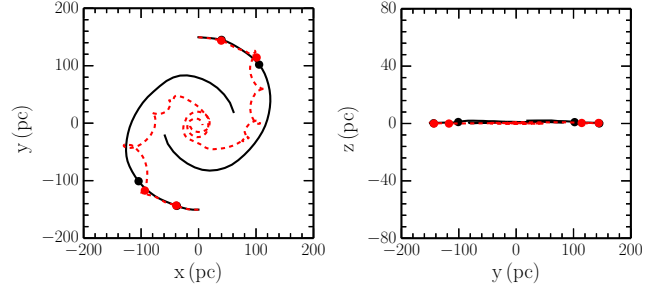


Figure 6. Same as figure 4 for the Noblast/SPH runs comparison.

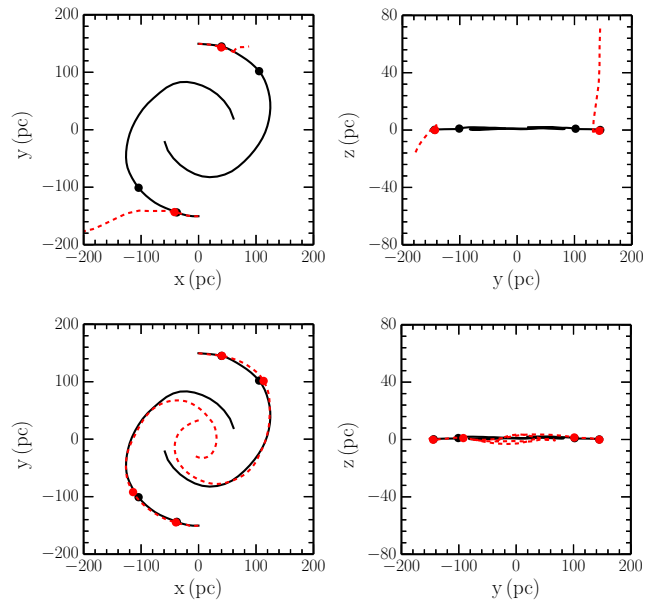


Figure 10. Same as figure 4 for the comparison between run SPH and runs Blast and Blast+.

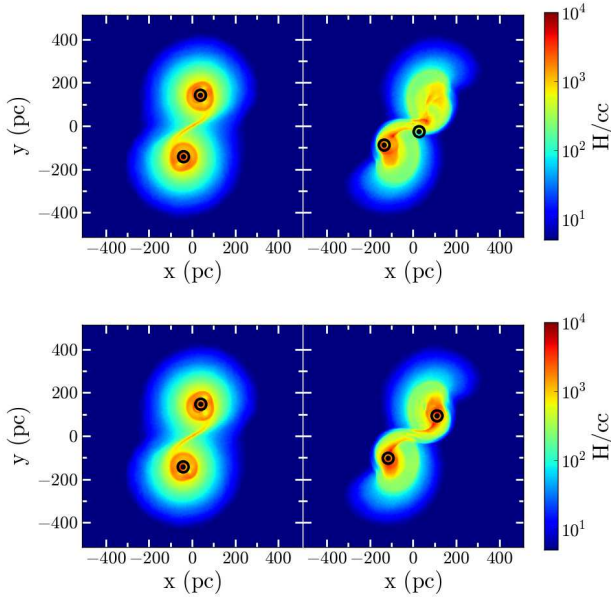


Figure 5. Upper panels: Gas density map at $t = 1$ Myr (left panels) and $t = 3$ Myr (right panels) for run Plain. The MBH positions are identified by the black bullseye symbols. Lower panel: same as upper panel for run Plain+.

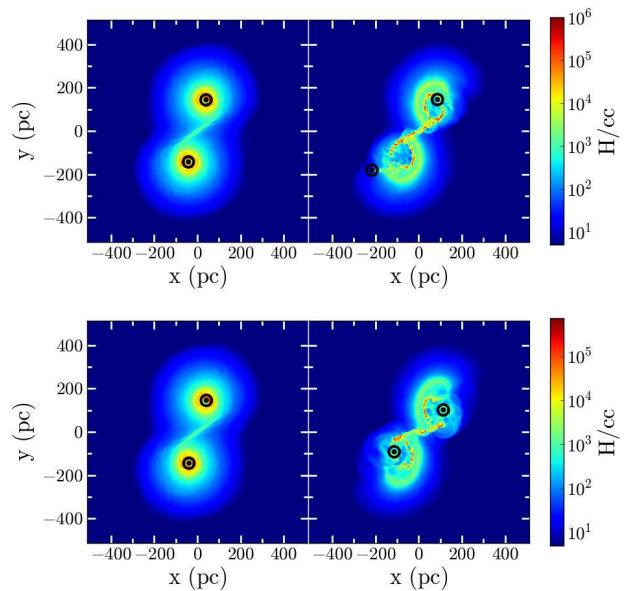


Figure 11. Same as figure 5 for runs Blast and Blast+.

of MBHs (Mayer et al. 2010; Ferrara, Haardt & Salvaterra 2013; Bonoli, Mayer & Callegari 2014).

5 ACKNOWLEDGEMENTS

We thank R. Teyssier and L. Paredi for many fruitful discussions. We acknowledge financial support from italian MIUR, through PRIN 2010-2011. We also acknowledge the CINECA award under the ISCRA initiative, for the availability of high performance computing resources and support. Part of the simulations were run on the LUCIA cluster at DiSAT, University of Insubria (Como).

REFERENCES

- Berger M. J., Colella P., 1989, *Journal of Computational Physics*, 82, 64
- Berger M. J., Olinger J., 1984, *Journal of Computational Physics*, 53, 484
- Binney J., Tremaine S., 2008, *Galactic Dynamics: Second Edition*. Princeton University Press
- Blecha L., Loeb A., Narayan R., 2013, *MNRAS*, 429, 2594
- Bonoli S., Mayer L., Callegari S., 2014, *MNRAS*, 437, 1576
- Callegari S., Kazantzidis S., Mayer L., Colpi M., Bellovary J. M., Quinn T., Wadsley J., 2011, *ApJ*, 729, 85
- Callegari S., Mayer L., Kazantzidis S., Colpi M., Governato F., Quinn T., Wadsley J., 2009, *ApJ*, 696, L89
- Chapon D., Mayer L., Teyssier R., 2013, *MNRAS*, 429, 3114
- Colpi M., Dotti M., 2011, *Advanced Science Letters*, 4, 181
- Consortium T. e. et al., 2013, *ArXiv e-prints*
- Daddi E. et al., 2010, *ApJ*, 714, L118
- Davies M. B., Miller M. C., Bellovary J. M., 2011, *ApJ*, 740, L42
- Di Matteo T., Springel V., Hernquist L., 2005, *Nature*, 433, 604
- Dotti M., Ruzkowski M., Paredi L., Colpi M., Volonteri M., Haardt F., 2009, *MNRAS*, 396, 1640
- Dotti M., Sesana A., Decarli R., 2012, *Advances in Astronomy*, 2012
- Dotti M., Volonteri M., Perego A., Colpi M., Ruzkowski M., Haardt F., 2010, *MNRAS*, 402, 682
- Dubois Y., Volonteri M., Silk J., 2014, *MNRAS*, 440, 1590
- Dubois Y., Volonteri M., Silk J., Devriendt J., Slyz A., 2014, *MNRAS*, 440, 2333
- Enßlin T. A., Pfrommer C., Springel V., Jubelgas M., 2007, *A&A*, 473, 41
- Escala A., Larson R. B., Coppi P. S., Mardones D., 2005, *ApJ*, 630, 152
- Ferrara A., Haardt F., Salvaterra R., 2013, *MNRAS*, 434, 2600
- Fiacconi D., Mayer L., Roškar R., Colpi M., 2013, *ApJ*, 777, L14
- Gabor J. M., Bournaud F., 2013, *ArXiv e-prints*
- Genzel R. et al., 2010, *MNRAS*, 407, 2091
- Hernquist L., 1990, *ApJ*, 356, 359
- Hobbs G. et al., 2010, *Classical and Quantum Gravity*, 27, 084013
- Hopkins P. F., Hernquist L., Hayward C. C., Narayanan D., 2012, *MNRAS*, 425, 1121
- Kormendy J., 2013, *Secular Evolution in Disk Galaxies*, Falcón-Barroso J., Knapen J. H., eds., p. 1
- Lupi A., Colpi M., Devecchi B., Galanti G., Volonteri M., 2014, *Monthly Notices of the Royal Astronomical Society*, 442, 3616
- Maio U., Dotti M., Petkova M., Perego A., Volonteri M., 2013, *ApJ*, 767, 37
- Mayer L., Kazantzidis S., Escala A., Callegari S., 2010, *Nature*, 466, 1082
- Rasera Y., Teyssier R., 2006, *A&A*, 445, 1
- Sesana A., Barausse E., Dotti M., Rossi E. M., 2014, *ArXiv e-prints*
- Springel V., 2005, *MNRAS*, 364, 1105
- Teyssier R., 2002, *A&A*, 385, 337
- Teyssier R., Pontzen A., Dubois Y., Read J. I., 2013, *MNRAS*, 429, 3068
- Van Wassenhove S., Volonteri M., Mayer L., Dotti M., Bellovary J., Callegari S., 2012, *ApJ*, 748, L7